Available online at www.sciencedirect.com

ScienceDirect

Procedia CIRP 138 (2026) 1207–1212

www.elsevier.com/locate/procedia

18th CIRP Conference on Intelligent Computation in Manufacturing Engineering

In-line Process Monitoring of Extrusion-Based Bioprinting Using In-Situ Thermal Imaging

Egon Prioglio[a], Giovanni Zanderigo[a], Bianca Maria Colosimo[a]*

[a]*Department of Mechanical Engineering, Politecnico di Milano, Via La Masa, 1, 20156, Milano, Italy*

*Corresponding author. E-mail address: biancamaria.colosimo@polimi.it

Abstract

In-situ monitoring is crucial in facilitating the industrial expansion of extrusion additive manufacturing by enabling the early detection of defects in a non-destructive manner and at a low cost. This study introduces a technique for assessing the geometric accuracy of extrusion additive manufacturing using a thermal camera as a sensor to monitor the extrusion-based bioprinting process in situ. The geometry of the extruded material is continuously detected during deposition, allowing for a real-time comparison with the corresponding nominal shape, which is extracted from the G-code and registered on the acquired thermal image sequences. The study demonstrates the effectiveness of the proposed in-line monitoring technique in identifying the correctly deposited material, the regions of under-extrusion and the regions of over-extrusion when printing with a transparent biomaterial.

Peer-review under responsibility of the scientific committee of the 18th CIRP Conference on Intelligent Computation in Manufacturing Engineering (CIRP ICME ‘24)

Keywords: In-line process monitoring; In-situ thermal imaging; Image-based defect detection; Extrusion-based bioprinting (EBB)

1. Introduction

Among the emerging additive manufacturing (AM) technologies, bioprinting aims at fabricating artificial organs and grafts by arranging living and non-living materials in a three-dimensional structure according to a distinct organization [1], [2]. Bioprinting shows the potential to disrupt the healthcare industry; indeed, it explores the opportunity to tackle the shortage of organ donors by producing artificial organs containing cells collected from the patient, minimizing the risk of rejection after transplantation [1], [2]. Bioprinting has also garnered attention from international space agencies to produce clinically applicable tissue grafts that can support autonomous medical treatment of astronauts in long-term space missions [3].

In academic and industrial settings, extrusion-based bioprinting (EBB) is the most diffused bioprinting technology [4]. The bioink, a formulation of soft biomaterials, is initially placed in a plastic cartridge and extruded from a nozzle in the shape of cylindric filaments to generate layer-by-layer the desired three-dimensional construct. EBB is likely the most scalable bioprinting technology thanks to its affordability, simplicity, versatility, and compatibility with a wide range of bioinks [2], [4]. Still, sub-optimal process parameters, construct design, and heterogeneous bioink properties cause material deposition defects that prevent the clinical adoption of EBB [5]. Indeed, accurate bioink deposition is essential to replicate the architecture of native tissues from a mechanical and biological standpoint [6]. Moreover, the stock of biomaterial is restricted, and constructs are patient-specific; therefore, random sampling of parts is not feasible [7]. For this

Peer-review under responsibility of the scientific committee of the 18th CIRP Conference on Intelligent Computation in Manufacturing Engineering (CIRP ICME ‘24)
10.1016/j.procir.2026.01.208

reason, in-situ process monitoring of EBB is essential to achieve an interior view of the printed part during construction in a non-destructive manner, detect material deposition errors, correct errors in-line, and identify optimal process parameters.

The literature has investigated in-situ monitoring of material deposition in EBB with various sensing technologies. In three studies, Armstrong et al. employed a displacement scanner to monitor, and correct in subsequent prints, the nozzle trajectory and the filament width [6], [8], [9]. Yang et al. developed a self-built optical coherence tomography probe mounted next to the nozzle to measure filament width and adjust process parameters in subsequent iterations to achieve the desired filament width. In the same study, Yang et al. assessed the undesired interruption of filaments by comparing the reconstructed profile of printed segments with their nominal geometry [10]. Zanderigo, Bracco et al. exploited images in the visible light spectrum to assess the quality of printed parts and build probabilistic printability maps to optimize process parameters starting from a small experimental campaign [11].

Nevertheless, the methods proposed in the literature measured the quality characteristics after printing a layer without evaluating their measure in line. Moreover, they did not demonstrate the compatibility of their methods with transparent bioinks. Bioprinting frequently adopts transparent bioinks, essential when printing parts mimicking specific tissues such as the cornea [12], [13]. However, monitoring in situ the quality of parts printed with a transparent biomaterial is challenging due to their optical properties. Bonatti et al. and Jin et al. proposed methods to evaluate the presence of defects in parts printed with a transparent bioink by employing a camera imager and machine learning methods, but these solutions did not encompass a geometric evaluation of the deposited material [14], [15].

Our previous work reported a proof of concept for in-line geometry reconstruction in EBB by adopting in-situ thermal imaging to monitor parts printed with a transparent bioink [16]. Regardless of its optical properties, the bioink flowing out from the extruder commonly has a temperature higher than the substrate. In thermal images, this phenomenon translates into a visible contrast between the biomaterial and the background inside a region of interest (ROI) next to the nozzle. Therefore, the extruder was motion-tracked to detect the location of the ROI at every time instant, and image segmentation was applied inside that region.

Building on these foundations, this study presents a robust method for monitoring the geometry of a transparent bioink during deposition utilizing an improved in-situ thermal imaging setup and the trajectory encoded in the G-code. A thermal camera was employed to record image sequences of the EBB process, and the G-code trajectory was aligned with the motion of the nozzle throughout a recorded image sequence to determine the position of the ROI. To represent ideal deposition, the nominal trajectory was interpolated with a circular shape where extrusion was expected. As extrusion took place, the shape of the deposited biomaterial was segmented inside the ROI to allow a continuous comparison between experimental and ideal deposition.

This paper is structured as follows: section 2 presents the bioprinting and in-situ thermal imaging setup. Section 3 explains the methods to process the collected thermal images and implement in-line monitoring. In section 4, the proposed methodology is discussed by highlighting strengths and limitations. Finally, in section 5, conclusions and an outlook on future work are redacted.

2. Process Sensing

2.1 *Bioprinting Platform*

To conduct bioprinting experiments, the pneumatic extrusion-based bioprinter named BIOX (Cellink, Gothenburg, Sweden) was utilized.

The pneumatic print-head temperature was set at 37°C, while the print-bed temperature was set at 18°C. A self-prepared transparent bioink was employed. Initially, an 8% (w/v) Sodium Alginate stock solution was obtained by dissolving Sodium Alginate (Sigma Aldrich, St. Louis, USA) in purified water. Before printing, to achieve the desired printability, 3 mL of the solution were pre-crosslinked with 1 mL of 0.136 molar solution of calcium chloride, resulting in a final concentration of Sodium Alginate at 6%.

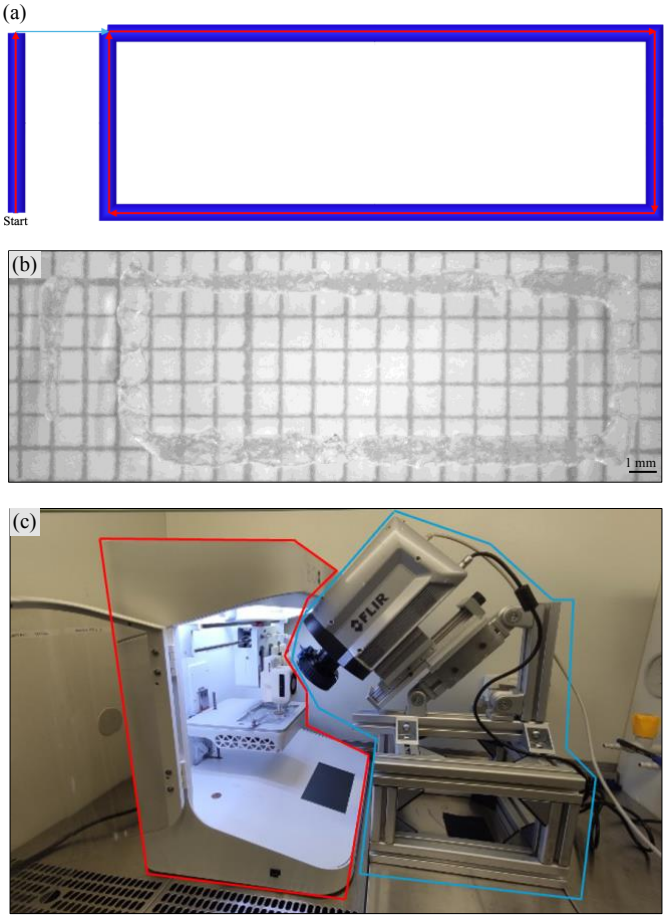

Figure 1: (a) G-code schematic indicating displacement with extrusion (red arrows) and without extrusion (blue arrows). (b) Example of a printed construct using transparent Alginate 6% bioink. The image was captured on graph paper background with a visible light camera. (c) Experimental setup featuring the BIOX extrusion-based bioprinter (left, red) and the X6900sc thermal camera on self-developed mount (right, blue).

Eventually, the biomaterial was loaded into a 3 mL plastic cartridge equipped with a conical nozzle ending with a diameter of 0.410 mm.

For printing, a personalized G-code was imported into the bioprinter (Figure 1(a)). The G-code was designed to print a single layer, consisting of a 5 mm straight filament placed at 2.5 mm to the left of the shortest side of the perimeter of a 15x5 mm rectangle. After conducting a small set of testing prints, extrusion pressure was set at 65 Kpa and nozzle traveling speed at 10 mm/s to obtain the desired filament diameter.

2.2 *In-situ Thermal Imaging*

The thermal camera employed for in-situ data collection was the X6900sc by Teledyne FLIR LLC (Wilsonville, U.S.). The X6900sc is an infrared radiation (IR) thermal imaging camera recording images of 640x512 pixels in sequences up to 1000 Hz. A thermal image sequence was recorded during each print with a frame rate limited to 30 Hz. This value was sufficiently high to avoid losing process information while containing the size of the digital files generated.

The thermal imaging camera was placed on a self-developed mount in front of the bioprinter. Top-view imaging was impeded by the encumbrance of the data sensing setup, so the camera was positioned at approximately 45° with respect to the print bed (Figure 1(c)).

The camera was coupled with a 50mm (f/2.5) lens supplied by the manufacturer. A 0.75-inch metallic extension ring was mounted between the camera and the lens, resulting in a magnified image with a spatial resolution of 55 µm/pixel. As a downside, the extender ring caused a restricted depth of field, imposing a boundary to the y-axis dimensions of the designed G-code. The extender ring also caused vignetting, a common undesirable phenomenon in thermal images caused by the interaction between the optics and the heat absorbed by the metal of the ring during camera operation [17]. Vignetting consists of a Gaussian-like gradient that extends from the center of the image to the edges. However, the camera depicted printed constructs in the central area of the frame, which was less affected by vignetting. In addition, although the thermal imaging camera did not capture true temperature values, it was able to detect a clear temperature contrast between the extruded biomaterial and the background.

3. Data Processing

3.1 Thermal Images Pre-Processing

Each acquired thermal image sequence was pre-processed considering the following steps:

• **Normalization:** since actual temperature values were not relevant for this study, the original thermal image sequence containing IR radiation count values was transformed with linear rescaling across all frames to obtain a greyscale representation that preserved the relative difference between pixel values. In greyscale, black corresponded to the lowest temperature, while white corresponded to the highest temperature.

• **Perspective adjustment**: the thermal imaging camera could not capture the deposited material with a top-view framing, thus requiring perspective adjustment of the acquired images. Perspective adjustment was necessary to correct perspective distortions and to align the acquired images with the orientation of the G-code coordinate system for future registration of the G-code trajectory on the captured thermal images. Within the first frame of the thermal image sequence, the operator manually identified the coordinates of four recognizable landmarks on the print-bed. Then, the utilized script computed the projective transformation required to align the landmarks' coordinates in the digital space with their coordinates in the real-world space. The script applied the obtained transformation to all frames. The *spatial resolution* (mm/pixel) was computed as the distance between landmarks in the real world divided by the distance between landmarks in the digital space.

• **Cropping**: to enhance processing efficiency, all frames in the thermal image sequence were cropped to a region in which material deposition occurred.

3.2 G-code Trajectory Extrapolation

To align the G-code trajectory to the pre-processed thermal image sequence, the following methods were applied:

• **G-code parsing**: the G-code used for bioprinting was imported into a self-developed parser script. The parser script converted the G-code text into a matrix where each row corresponded to a movement command and the columns reported the corresponding *x-target position* (mm), *y-target position* (mm), *displacement speed* (mm/s) and *extrusion* (either 1 or 0) during displacement.

• **G-code trajectory computation:** a second script generated the G-code trajectory by processing row by row the matrix created by the parser script. Initially, the script converted the *x-target position* and the *y-target position* from mm to pixel, and the *displacement speed* from mm/s to pixel/s by exploiting the *spatial resolution* (mm/pixel). Then, the code computed the *displacement distance* (pixel) between the *current position (x, y)*, initialized at (0,0), and the *target position (x-target, y- target)* using the Euclidean distance. The script computed the *time to move* (s) from the *current position* to the *target position* by considering the *displacement distance* and the *displacement speed*, as well as the *acceleration* (pixel/s^2) and *deceleration* (pixel/s^2) of the extruder at starting, ending, and turning points. The *time to move* (s) was multiplied by the acquisition *frame rate* (Hz) to obtain the *number of frames* required to complete the displacement. At this point, both for the x-axis and the y-axis, a linearly spaced vector covering the *displacement distance* from the *current position* to the *target position* was generated considering the *number of frames* required for completing the move command so that for each frame in the thermal image sequence a *trajectory point (x, y, frame number, extrusion, direction)* existed. For each *trajectory point*, the *extrusion* binary value, necessary to determine if extrusion should occur or not it those coordinates according to the move command extrapolated from the G-code, was stored.

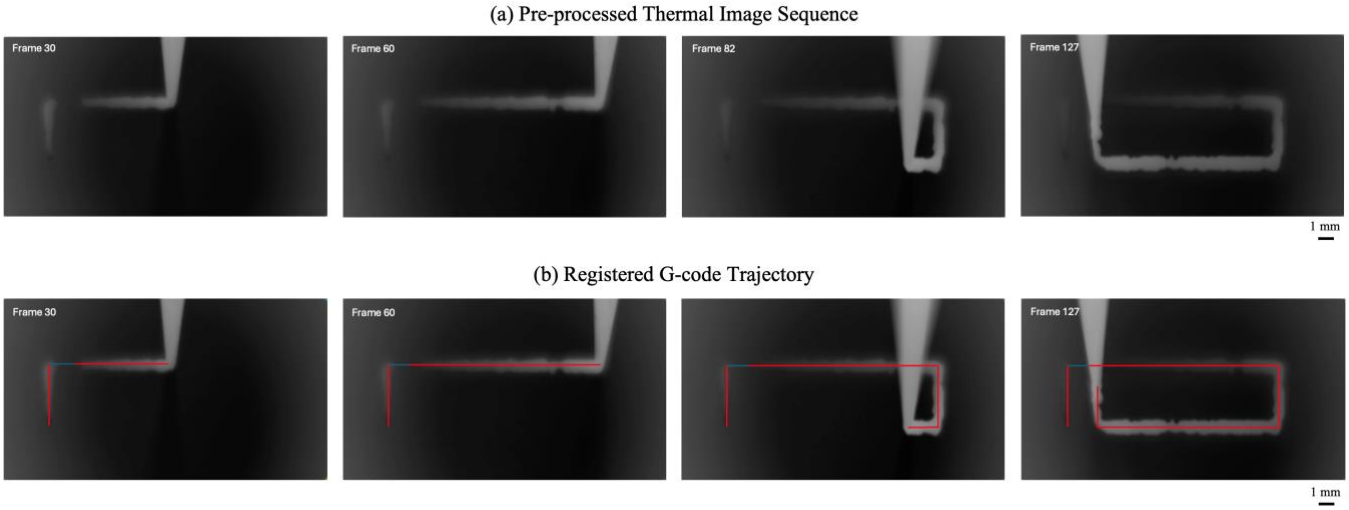

Figure 2: Frames 30, 60, 82 and 127 of thermal image sequence. In greyscale, black corresponds to the lowest temperature, while white corresponds to the highest temperature. (a) Pre-processed frames. (b) Registered G-code trajectory schematic indicating displacement with extrusion (red segments) and without extrusion (blue segments).

Eventually, the *direction* (°) of the trajectory for each *trajectory point* was also stored based on the change in *x* and *y* coordinates from one frame to the next.

The overall nominal trajectory was generated by concatenating the trajectory generated for each G-code movement command.

• **G-code trajectory registration:** as discussed, the developed script generated the G-code trajectory according to the image-wise coordinate system of the acquired thermal images, and it generated one trajectory point for each recorded frame. The G-code trajectory starting position was initialized at the origin (0,0), but the positioning of the extruder in the thermal images at the beginning of the G-code execution was different. To align the G-code trajectory with the position of the nozzle in the acquired images, the *x* and *y* coordinates of all trajectory points were shifted according to the relative position between the nozzle tip and the origin at the start of the G-code. The position of the nozzle tip was manually identified in the frame where the bioprinter began executing the G-code.

3.3 Thermal Images Segmentation

The proposed image segmentation approach encompassed three main steps to segment the shape of the transparent biomaterial during deposition:

• **Region of interest (ROI) detection:** during extrusion, the deposited material had a temperature higher than the substrate in a region next to the nozzle defined as the region of interest (ROI). Then, the temperature of the deposited bioink decreased until it matched the temperature of the print-bed. From a thermal imaging perspective, inside the ROI, a significant contrast between the background and the bioink was detected, regardless of the transparency of the material. Instead, outside of the ROI, this contrast decreased as time passed after deposition. For this reason, to segment the shape of the extruded material, the ROI was detected in every frame of the pre-processed thermal image sequence (Figure 3(a)).

During each frame processing, an automatic script generated an image mask to black out all the pixels in the image except those contained in the ROI. The ROI positioning was defined by the G-code trajectory, so that the *trajectory point* at that instant was at the center of one of its sides, and the ROI extended in the opposite direction to the direction in which the extruder was moving. The ROI was sized to ensure that material deposition occurred inside it. Since the ROI included a portion of the nozzle, an additional trapezoid mask was generated to cover it in all frames. The utilized script automatically placed the trapezoid mask in every frame, knowing its relative position with respect to the *trajectory point*.

When the extruder moved toward the thermal camera, with a *direction* of 270º, the nozzle obscured the deposited bioink in the acquired thermal images. Therefore, if the *direction* associated with a *trajectory point* was 270º, the ROI was not placed, and no segmentation occurred. Then, when a new frame with a different *direction* associated with the *trajectory point* came up, the ROI for that frame was composed of the region of interest corresponding to the *trajectory point* in the new frame and in all those frames in which the nozzle impeded visibility. This procedure enabled visibility on the obscured bioink before the complete cooling of the biomaterial.

• **Otsu's thresholding:** after detecting the ROI, the developed script adjusted the contrast inside it, and the shape of the deposited material could be segmented from the background utilizing Otsu's thresholding (Figure 3 (b)).

• **Segmented profile generation:** since each ROI contained the bioink extruded at a specific time instant, the overall segmented profile of the printed part was derived by concatenating all the segmented filaments accumulated until that time (Figure 3 (c)).

3.4 In-line Process Monitoring

After obtaining the cumulative segmented profile of the extruded bioink up to the currently processed frame, the shape

of the experimental deposition was compared to the deposition expected from the G-code.
For this purpose, the utilized script interpolated the G-code trajectory with a circle, with a radius equivalent to half the desired diameter of the deposited bioink, in those trajectory points where the G-code imposed to extrude (Figure 3 (d)).
A color-coded image was generated to depict the matching and mismatching between the shapes representing experimental and ideal deposition. The intersection between desired and obtained deposition was green (correct extrusion), the regions in which the G-code imposed extrusion but it did not occur were blue (under-extrusion), and the regions in which extrusion was not imposed but material was deposited were red (over-extrusion) (Figure 3 (e)).

4. Discussion

In-line defect detection in extrusion-based bioprinting (EBB) is essential to preserve the limited stock of biomaterial and enable strategies for adjusting process parameters and enhancing quality in real-time. This study proposes a solution for in-line monitoring of EBB utilizing in-situ thermal imaging and the information encoded in the G-code.
The experiment conducted showed that thermal imaging was appropriate to detect the geometry of a transparent biomaterial during extrusion. However, the resolution of thermal imagers is a limiting factor compared to sensors working in the visible field of light. In our previous work, the thermal imaging setup yielded a spatial resolution of 200 um/pixel.

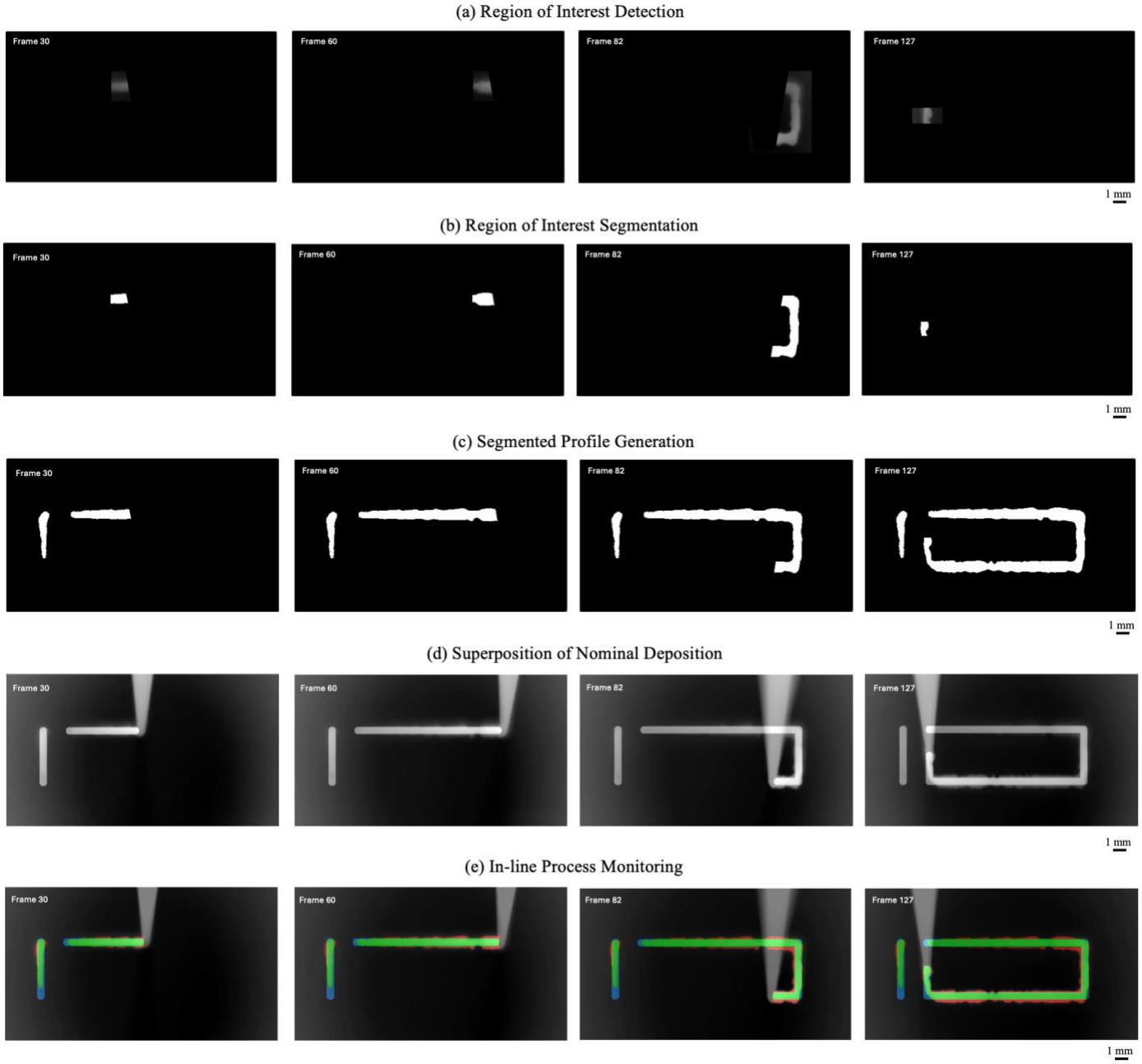

Figure 3: Frames 30, 60, 82 and 127 of thermal image sequence. In greyscale, black corresponds to the lowest temperature, while white corresponds to the highest temperature. (a) Region of interest detection. Frame 82 exemplifies the placement of the ROI to reveal the shape of extruded material previously obscured by the nozzle's motion towards the thermal imaging camera. (b) Region of interest segmentation. (c) Segmented profile generation. The segmented profile was generated by concatenating up to the current frame the segmented profiles of the regions of interest detected in the previous frames. (d) Superposition of nominal deposition. The nominal deposition was obtained by interpolating the G-code trajectory with a circle of appropriate radius in those trajectory points where the G-code imposed to extrude. (e) In-line process monitoring. The experimental and nominal deposition shapes were compared. The color-coded images show correct deposition in green, over-extrusion in red, and under-extrusion in blue.

In this paper, the thermal imaging setup was upgraded by mounting the 0.75-inch extender ring between the camera and the lens, reaching a spatial resolution of 55 um/pixel after perspective adjustment. The setup improvement allowed an accurate segmentation of small features in the deposited biomaterial. Nevertheless, the setup produced a depth of field of less than 10 mm. This characteristic wouldn't have limited the design of printed parts if imaged with a top-view framing, given that the layer height was 0.410 mm, but on-axis framing was impeded by the dimensions of the camera and the design of the bioprinter. Since the camera had a 45° tilt angle with respect to the print-bed, the y-axis dimensions of printed parts were bound to 5 mm to ensure that they were in focus. Vignetting was another technical problem caused by the extender ring. However, keeping the monitored part in the central region of the acquired images and independently processing the pixels in the ROI produced stable segmentation results.

Our previous work employed motion tracking to determine the position of the nozzle and, consequently, the ROI. In this work, the computational effort required by motion tracking was avoided by extrapolating the extruder trajectory from the inherent information of the G-code. The registered G-code trajectory could determine the position of the nozzle tip in a stable and accurate way. In addition, unlike motion tracking, the registered G-code trajectory could predict where material deposition was expected or not along the printing path. For this reason, the new approach identified in-line the correctly deposited material, the regions of under-extrusion, and the regions of over-extrusion. The direct correlation between the detected defects and their spatial position given by the G-code trajectory is an enabler for future implementation of feedback-loop control, in which process parameters are adjusted in line to obtain the ideal deposition.

5. Conclusions

The developed study highlights the relevance of in-situ monitoring in EBB to assess the fidelity of printed constructs in a non-destructive manner during construction. By leveraging in-situ thermal imaging alongside the information embedded in G-code, the proposed method offers a robust solution for in-line segmentation of the deposited biomaterial, even when a transparent bioink is deposited. Through this approach, the correctly deposited material, as well as regions of under-extrusion and over-extrusion were identified along the printing trajectory.

Future work will build on these results to evaluate the accuracy of in-line image segmentation through in-situ thermal images against alternative sensors. In addition, future efforts will focus on assessing in line the geometry of the segmented profile by measuring the filament width along the printing path. Eventually, by studying the relationship between process parameters and filament width, future research will aim at developing feedback-loop control to enhance the quality of parts during printing to pursue defect-free and zero-waste biofabrication.

Acknowledgements

This research was partially funded by the European Commission under the “HORIZON-CL4-2021-DIGITAL-EMERGING-01 project BioProS - Biointelligent Production Sensor to Measure Viral Activity” (grant agreement no. 101070120), 2022-2026”.

References

[1] S. Santoni, S. G. Gugliandolo, M. Sponchioni, D. Moscatelli, and B. M. Colosimo, “3D bioprinting: current status and trends—a guide to the literature and industrial practice,” *Bio-Design and Manufacturing*, vol. 5, no. 1. Springer, pp. 14–42, Jan. 01, 2022. doi: 10.1007/s42242-021-00165-0.

[2] K. Shinkar and K. Rhode, “Could 3D extrusion bioprinting serve to be a real alternative to organ transplantation in the future?,” *Annals of 3D Printed Medicine*, vol. 7, p. 100066, Aug. 2022, doi: 10.1016/j.stlm.2022.100066.

[3] A. Van Ombergen *et al.*, “3D Bioprinting in Microgravity: Opportunities, Challenges, and Possible Applications in Space,” *Adv Healthc Mater*, vol. 12, no. 23, p. 2300443, Sep. 2023, doi: 10.1002/ADHM.202300443.

[4] I. Matai, G. Kaur, A. Seyedsalehi, A. McClinton, and C. T. Laurencin, “Progress in 3D bioprinting technology for tissue/organ regenerative engineering,” *Biomaterials*, vol. 226. Elsevier Ltd, Jan. 01, 2020. doi: 10.1016/j.biomaterials.2019.119536.

[5] C. Liu *et al.*, “Computer vision-aided bioprinting for bone research,” *Bone Research*, vol. 10, no. 1. Springer Nature, Dec. 01, 2022. doi: 10.1038/s41413-022-00192-2.

[6] A. A. Armstrong, J. Norato, A. G. Alleyne, and A. J. Wagoner Johnson, “Direct process feedback in extrusion-based 3D bioprinting,” *Biofabrication*, vol. 12, no. 1, 2020, doi: 10.1088/1758-5090/ab4d97.

[7] B. Schmieg, S. Gretzinger, S. Schuhmann, G. Guthausen, and J. Hubbuch, “Magnetic resonance imaging as a tool for quality control in extrusion-based bioprinting,” *Biotechnol J*, vol. 17, no. 5, May 2022, doi: 10.1002/biot.202100336.

[8] A. A. Armstrong, A. G. Alleyne, and A. J. Wagoner Johnson, “1D and 2D error assessment and correction for extrusion-based bioprinting using process sensing and control strategies,” *Biofabrication*, vol. 12, no. 4, Oct. 2020, doi: 10.1088/1758-5090/aba8ee.

[9] A. A. Armstrong, A. Pfeil, A. G. Alleyne, and A. J. Wagoner Johnson, “Process monitoring and control strategies in extrusion-based bioprinting to fabricate spatially graded structures,” *Bioprinting*, vol. 21, Mar. 2021, doi: 10.1016/j.bprint.2020.e00126.

[10] S. Yang, L. Wang, Q. Chen, and M. Xu, “In situ process monitoring and automated multi-parameter evaluation using optical coherence tomography during extrusion-based bioprinting,” *Addit Manuf*, vol. 47, Nov. 2021, doi: 10.1016/j.addma.2021.102251.

[11] G. Zanderigo, F. Bracco, Q. Semeraro, and B. M. Colosimo, “In-situ Printability Maps (IPM): A new approach for in-situ printability assessment with application to extrusion-based bioprinting,” *Bioprinting*, vol. 36, p. e00320, Dec. 2023, doi: 10.1016/J.BPRINT.2023.E00320.

[12] M. Hospodiuk, M. Dey, D. Sosnoski, and I. T. Ozbolat, “The bioink: A comprehensive review on bioprintable materials,” *Biotechnol Adv*, vol. 35, no. 2, pp. 217–239, Mar. 2017, doi: 10.1016/J.BIOTECHADV.2016.12.006.

[13] H. Kim, M. N. Park, J. Kim, J. Jang, H. K. Kim, and D. W. Cho, “Characterization of cornea-specific bioink: high transparency, improved in vivo safety,” *J Tissue Eng*, vol. 10, Jan. 2019, doi: 10.1177/2041731418823382.

[14] A. F. Bonatti, G. Vozzi, C. Kai Chua, and C. De Maria, “A deep learning approach for error detection and quantification in extrusion-based bioprinting,” *Mater Today Proc*, Jan. 2022, doi: 10.1016/j.matpr.2022.09.006.

[15] Z. Jin, Z. Zhang, X. Shao, and G. X. Gu, “Monitoring Anomalies in 3D Bioprinting with Deep Neural Networks,” *ACS Biomater Sci Eng*, 2021, doi: 10.1021/acsbiomaterials.0c01761.

[16] B. M. Colosimo, S. G. Gugliandolo, E. Prioglio, and D. Moscatelli, “International Journal of Bioprinting A new solution for in situ monitoring of shape fidelity in extrusion-based bioprinting via thermal imaging,” *Int J Bioprint*, 2024, doi: 10.36922/ijb.2021.